Fermi surface topology and low-lying electronic structure of a new iron-based superconductor $Ca_{10}(Pt_3As_8)(Fe_2As_2)_5$

M. Neupane*,[1] Chang Liu*,[1] S.-Y. Xu,[1] Y. J. Wang,[2] N. Ni,[3] J. M. Allred,[3]
L. A. Wray,[1,4] H. Lin,[2] R. S. Markiewicz,[2] A. Bansil,[2] R. J. Cava,[3] and M. Z. Hasan[1]

[1]*Joseph Henry Laboratory and Department of Physics, Princeton University, Princeton, New Jersey 08544, USA*
[2]*Department of Physics, Northeastern University, Boston, Massachusetts 02115, USA*
[3]*Department of Chemistry, Princeton University, Princeton, New Jersey 08544, USA*
[4]*Advanced Light Source, Lawrence Berkeley National Laboratory, Berkeley, California 94305, USA*

(Dated: October 24, 2011)

We report a first study of low energy electronic structure and Fermi surface topology for the recently discovered iron-based superconductor $Ca_{10}(Pt_3As_8)(Fe_2As_2)_5$ (the 10-3-8 phase, with $T_c \sim 8$ K), via angle resolved photoemission spectroscopy (ARPES). Despite its triclinic crystal structure, ARPES results reveal a fourfold symmetric band structure with the absence of Dirac-cone-like Fermi dots (related to magnetism) found around the Brillouin zone corners in other iron-based superconductors. Considering that the triclinic lattice and structural supercell arising from the Pt_3As_8 intermediary layers, these results indicate that those layers couple only weakly to the FeAs layers in this new superconductor at least near the surface, which has implications for the determination of its potentially novel pairing mechanism.

PACS numbers: 74.25.Jb, 74.70.Dd, 79.60.Bm

The recent discovery and characterization of new superconducting phases in the Ca-Fe-Pt-As system $Ca_{10}(Pt_nAs_8)(Fe_2As_2)_5$ [1–4] has potentially significant impact on the field of iron-based high-T_c superconductors [5–9]. Most importantly, these new phases serve as ideal platforms for systematic studies of the physics of the intermediary layers and their impact on the superconducting properties - an important yet open question in the field of arsenide superconductivity. In high-T_c cuprates [10–14], such a study is made possible by the availability of e.g. the $Bi_2Sr_2Ca_{n-1}Cu_nO_{2n+4+x}$ ($n = 1$ - 3) series [13, 14], within which one finds a drastic correlation between the number of intermediary layers and the superconducting transition temperature (T_c). In the iron pnictides, a similar type of survey has previously been unavailable due to the lack of appropriate systems: one needs to search for a series of stoichiometric materials with different but systematically adjusted chemical compositions in either the iron-containing layers or the intermediary layers. The unique crystal structures in the Ca-Fe-Pt-As systems, on the other hand, yield drastically different symmetries and periodicities for the layers of FeAs tetrahedra and the intermediary layers. Therefore, the intralayer (hopping within the FeAs layers) and interlayer (hopping between the FeAs and Ca-Pt-As layers) contribution to the density of states at the Fermi level (E_F) can be uniquely distinguished. Studies of the electronic structure of the Ca-Fe-Pt-As system are thus of crucial importance toward the understanding of the interlayer physics and the microscopic mechanism of high-T_c superconductivity in the iron pnictides.

In this paper, we report a study of the electronic structure of the Ca-Fe-Pt-As system for $n = 3$ [the 10-3-8 phase with $T_c \sim 8$ K, see Fig. 1(e)] using angle resolved photoemission spectroscopy (ARPES) as well as first principle calculations. ARPES measurements re-

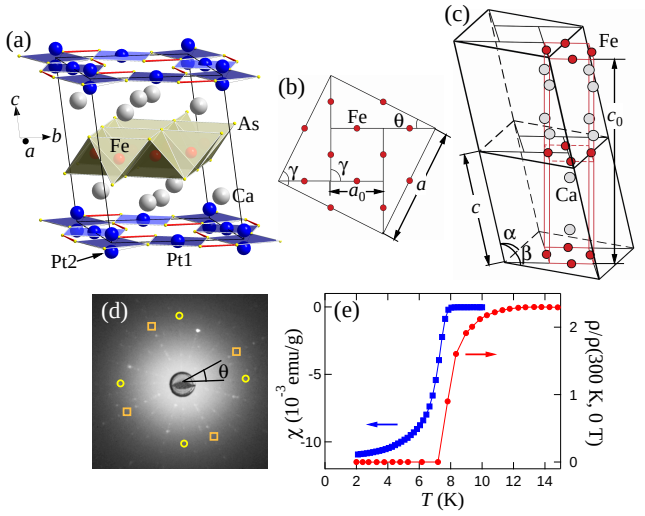

FIG. 1: Crystallographic and superconducting properties of $Ca_{10}(Pt_3As_8)(Fe_2As_2)_5$ (10-3-8). (a) Crystal structure of the 10-3-8 phase. (b)-(c) Schematic crystal structure in (b) the a-b plane and (c) three dimensions. (d) Laue picture of a 10-3-8 single crystal. Reflection peaks for both the triclinic (yellow circles) and tetragonal (orange squares) lattices are clearly observed. (e) Low temperature resistivity (right axis) and magnetic susceptibility (left axis) for the 10-3-8 phase.

*These authors contributed equally to this work.

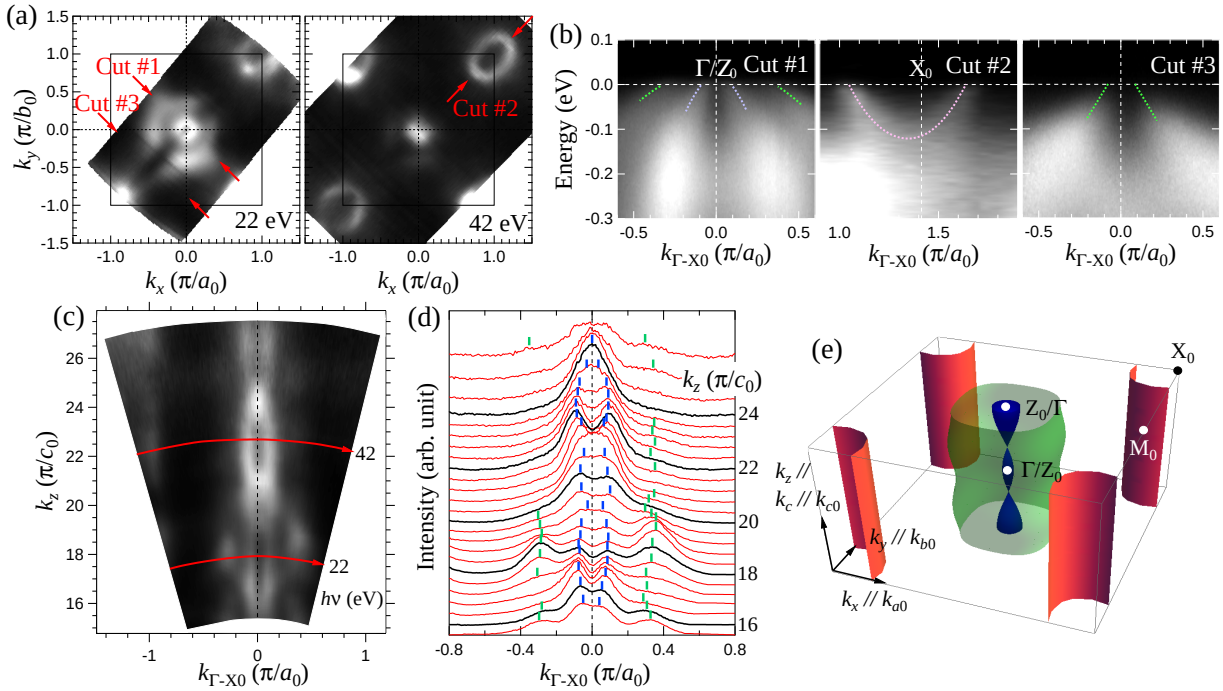

FIG. 2: Three dimensional (k_z dispersion) ARPES Fermi surface topology. (a) Fermi surface maps for two different photon energies (lower right corner in each panel). Brillouin zone sizes are determined based on the tetragonal cell [see Fig. 2(e) for relations between momenta in the triclinic and tetragonal cells]. (b) Raw k-E maps along directions marked by Cut #1 - #3 in Fig. 2(a). The two hole pockets around Γ/Z_0 and the electron pocket around X_0 are labeled as α_1, α_2 and β_1, respectively and are tracked with blue, green and pink colors. (c) k_z dispersion data for the 10-3-8 phase, taken along the Γ-X_0 direction with photon energies 15 to 64 eV. Inner potential is set to be 9.5 eV. (d) Momentum distribution curves (MDCs) for different k_z values. Fermi crossing bands are marked with the same colors as in Fig. 2(b). (e) Schematic experimentally-derived Fermi surface construction in three dimensions.

veal the three dimensional Fermi surface topology and the band structure close to E_F. We observe well defined Fermi surfaces with *tetragonal* symmetry that are similar to other iron-based superconductors, even though arising from an unambiguously triclinic crystal structure with a larger in-plane unit cell. First principle band calculations find very small contribution of the platinum density of states at E_F for the 10-3-8 phase. These results are indicative of a weak interlayer hopping between the FeAs and the PtAs intermediary layers in this Ca-Fe-Pt-As system. ARPES data also shows that the quasi nesting condition between the Fermi pockets at the Brillouin zone (BZ) center and the BZ corner is not perfect. This may be another reason for the low T_c of the 10-3-8 phase.

We begin our discussion with a detailed examination of the crystallographic properties of the 10-3-8 single crystal, as summarized in Fig. 1. This crystal has a triclinic unit cell with primitive vectors of length $a = b = 8.759$ Å, $c = 10.641$ Å, $\alpha = 94.744°$, $\beta = 104.335°$, and $\gamma = 90.044° \simeq 90°$ [2] [see Fig. 1(a)-(c) for definitions]. Markedly, such a triclinic atomic arrangement is experienced only by the platinum atoms in the crystal; the calcium atoms and the $FeAs_4$ tetrahedra arrange in a tetragonal fashion with lattice parameters $a_0 = b_0 = 3.917$ Å, $c_0 = 20.548$ Å. From Fig. 1(b) one notices that the in-plane triclinic unit cell is essentially a $\sqrt{5}$ superlattice that forms along the (210) direction of the tetragonal cell, making an in-plane inclusion angle of $\theta = \arctan(1/2) = 26.56°$ and a length relation $a = \sqrt{5}a_0$ between the two lattices. Fig. 1(c) reveals that the top and bottom surface centers of the triclinic unit cell displace horizontally via an in-plane vector $(a_0/2, a_0/2)$. Therefore the height of the tetragonal cell measures $c_0 = 2\sqrt{c^2 - a_0^2/2} = 20.548$ Å. Hence, if the interlayer hopping between the PtAs and FeAs layers is weak, the ARPES Fermi surface should reflect a similar topology to the other prototype pnictides, with possibly weak FeAs shadow bands associated with superlattice folding and additional features associated with the PtAs layer. It is important to point out that any potential crystal twinning would not hinder the ARPES observation of the PtAs superlattice. See online supplementary information (SI) for the detailed description of Fig. 1(d). From the present experiments, we cannot rule out the possibility that subtle surface reconstruction gives rise to a surface-driven electronic structure which has higher symmetry than that of the bulk.

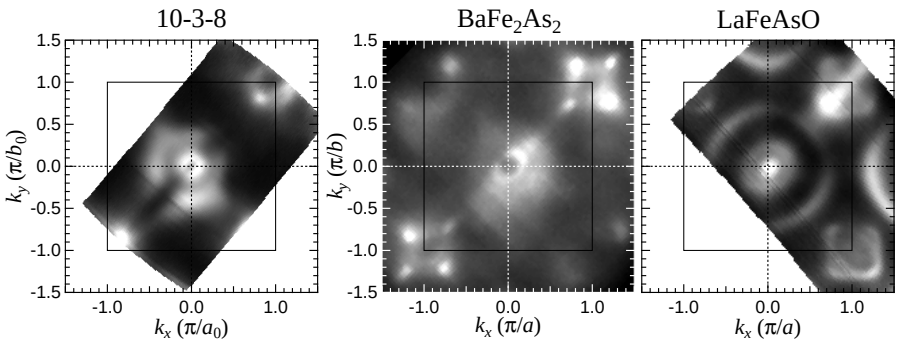

FIG. 3: Comparison of in-plane ARPES Fermi surfaces of the 10-3-8 phase, $BaFe_2As_2$ [23] and LaFeAsO [24]. Incident photon energies are 22, 105 and 45 eV, respectively. The Fermi "dots" seen around the X pockets of $BaFe_2As_2$ come from antiferromagnetic reconstructions of the electronic structure [23], and the large Γ hole pocket in LaFeAsO originates from surface effects [24].

We now present the ARPES data for the Fermi surface topology of the 10-3-8 phase. Fig. 2 shows the three dimensional electronic structure obtained by ARPES and a schematic three dimensional Fermi surface structure deduced from our experiments (see SI for a detailed description). The most important observation from Fig. 2 is that the ARPES electronic structure has a *tetragonal* symmetry, and the experimental Brillouin zone size is proportional to π/a_0 rather than π/a in the k_x-k_y plane [Fig. 2(a)]. In other words, the ARPES signal reveals that the electronic system is tetragonal at least near the surface, with the periodicity of the FeAs layer sublattice. This observation is noteworthy for two reasons. First, it points out directly that the triclinic arrangement and larger supercell periodicity of the platinum atoms has very little influence on the electronic structure; if the platinum orbitals had a strong contribution at E_F, then the observation of Fermi pockets arranged according to the triclinic Brillouin zone is expected - similar to what is shown in Fig. 4(c). From this we deduce that the hybridization between bands from the PtAs intermediary layers and those from the FeAs layers has to be weak. Although this is only a qualitative statement, the unique crystal structure of the 10-3-8 phase does provide an important estimation of the interlayer hopping strength that is otherwise hard to obtain from experiment in the Fe-As superconductors: interlayer hopping must be so weak that it renders the triclinic lattice invisible by photoemission. Second, the ARPES electronic structure mimics the electronic structures of other prototype pnictides like $AEFe_2As_2$ ("122", AE = Ca, Sr, Ba, etc.). Not only the in-plane lattice parameter a_0 but also the shapes, sizes and Fermi velocities of the Γ and X_0 Fermi pockets show very little difference with those for the 122 parent compounds [15–20] (see SI). This indicates that a universal electronic structure capturing the underlying superconducting mechanism may exist for different sub-families of the Fe-based superconductors (except for the $K_\alpha Fe_{2-\beta}Se_2$ series [21, 22]).

Despite the overall similarity, there are observable differences between the Fermi surface of the 10-3-8 phase and that of the prototype pnictides. In Fig. 3 we compare explicitly the in-plane ARPES Fermi surfaces for the 10-3-8 phase, $BaFe_2As_2$ [23] and LaFeAsO [24]. First, the Dirac-cone-like Fermi dots around the X points in $BaFe_2As_2$ are absent in the 10-3-8 phase [seen most clearly in the 42 eV panel of Fig. 2(a)]. Since these dots are direct consequences of the long range antiferromagnetic order present in the 122 compound [23, 25], their absence is consistent with the absence of an antiferromagnetic signature in transport measurements up to room temperature [2]. Second, extended ARPES intensity along one of the Γ-X_0 directions is seen only for the 10-3-8 phase. A close look into the k-E maps (data of Cut #3 in Fig. 2) reveals that there is an actual Fermi crossing in these locations, and that the band is holelike. We point out here that this band also originates from the Fe orbitals, since it shows reflective symmetry along the high symmetry directions of the iron unit cell rather than the triclinic platinum cell. Third, from the k_z dispersion data [Fig. 2(c)-(d)], one notices that ellipsoidal hole pockets are observed around both the Γ and Z_0 points for the 10-3-8 phase, while in the 122 parent compounds only Z ellipsoids are observed [18, 19]. According to band calculation (Fig. 4), this signifies the weak but existent Pt influence on the Fermi surface topology. The nesting condition for the Γ/Z_0 hole pockets and the X electron pockets is reasonable but not perfect; this may as well be a reason for the relatively low T_c detected.

We now examine the electronic structure of the Ca-Fe-Pt-As system from results of first principle calculations [26–28]. In the calculation, spin-orbit coupling effects are not included and E_F is fixed assuming zero electron doping. The crystal structure of the 10-3-8 phase is taken from Ref. [2] with the off-plane Pt (Pt2) atom in the (Pt_3As_8) layer assigned to one of its two possible positions - slightly above the plane [2] (see also SI). We show in Fig. 4(a) the calculated curves for the total density of states (DOS) as well as the partial DOS (PDOS) for the two different kinds of platinum atoms [Pt1 and Pt2, see Fig. 1(a)]. Similar to the prototype pnictides, the DOS in vicinity of E_F for the 10-3-8 phase is dominated by Fe 3d orbitals. In Fig. 4(b)-(c), the calculated LDA band structure and Fermi surface are shown in the triclinic Brillouin zone. From Fig. 4(b) we see that the innermost Γ band has stronger k_z dispersion than the

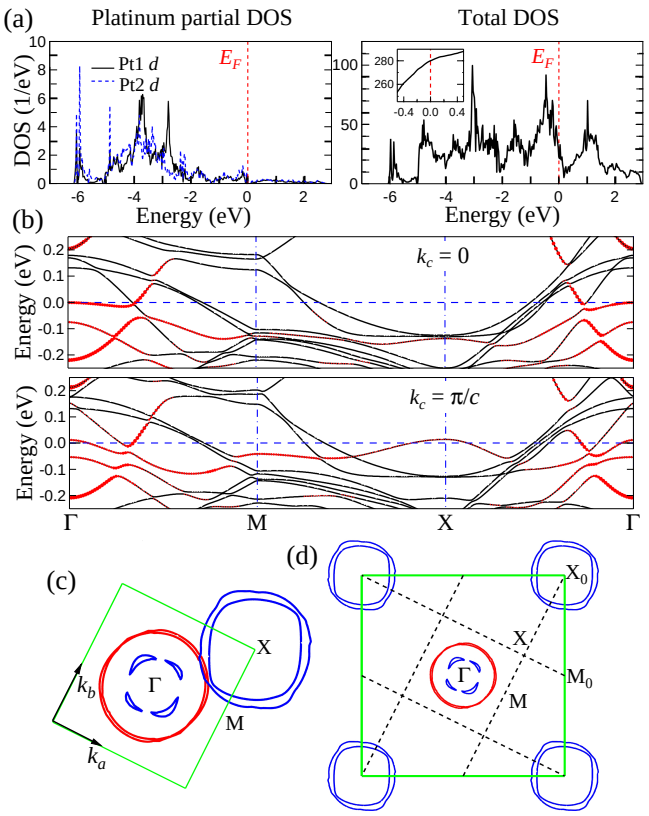

FIG. 4: Results of first principle calculations. (a) Calculated density of states (DOS) for the 10-3-8 phase. Left column: partial DOS for in-plane and out-of-plane platinum 5d orbitals (Pt1 & Pt2, respectively). Right column: Total DOS for all elements. Inset shows the integrated DOS (IDOS) near E_F. (b) Calculated band structure of 10-3-8 in the triclinic Brillouin zone. Red dots indicate the contribution of platinum orbitals. (c) Fermi surfaces sketched in the triclinic zone. (d) Fermi surfaces unfolded into the tetragonal zone.

other two holelike iron bands, which is consistent with the ARPES observations [Fig. 2(c)-(e)]. This band is hybridized with the Pt d_{xz} orbitals. Since the experimental data reveal no sign of the triclinic Fermi surfaces, we assume that the potential from the $\sqrt{5}$ superlattice arising from the Pt_3As_8 layers is very weak, in which case we can approximately "unfold" the LDA superlattice band structure into the tetragonal BZ, as shown in Fig. 4(d). The tetragonal Γ, X_0 and M_0 points form a subset of the supercell Γ, X and M points, so we systematically "erase" all superlattice FS maps not associated with the tetragonal symmetry points. From Fig. 4(d), we see that this process works well for the Fe Fermi surfaces, reproducing the familiar 122 structure. The fate of the electronlike Pt-bands (the four pedal-like small pockets near Γ) under this unfolding process is less clear, but it should be noted that these pockets are not clearly distinguished by ARPES.

Interlayer hopping plays an important role in the presence of high-T_c superconductivity in both the cuprates and the Fe-based superconductors. It is believed that the hopping strength in the prototype pnictides is somewhat stronger than that in the cuprates (although still on the weak side), and that this may lead to the differences between T_c and pairing symmetry in these two families. Zhai *et al.* propose that the superconducting gap symmetry changes from d-wave to s-wave with increasing hopping strength [29]. Although the model in Ref. [29] may not apply directly to the Ca-Fe-Pt-As systems, where spin density wave signatures have not yet been detected at low temperatures, it is likely that the unique momentum-space separation of the inter- and intra-layer signals in the 10-3-8 system helps to determine the hopping strength with considerably higher accuracy, thus shedding light on the ultimate determination of the superconducting mechanism in both classes of high-T_c superconductors.

In conclusion, we have presented a systematic study of the band structure and Fermi surfaces of one of the new Ca-Fe-Pt-As superconductors in the vicinity of E_F. Our ARPES observation - reduced tetragonal electronic structure and little k_z dispersion - points to a weak interlayer hopping strength in this system. The Dirac-cone-like Fermi dots around X are absent in the 10-3-8 phase, consistent with the absence of long range antiferromagnetism in this compound. The nesting condition between the Fermi pockets at the center and the corners of the Brillouin zone is not perfect. This may contribute to the low T_c of the 10-3-8 phase. First principle calculations agree well with experimental data if the potential from the $\sqrt{5}$ superlattice arising from the PtAs layers is considered to be very weak, and the triclinic band structure can be unfolded onto the tetragonal Brillouin zone. The Ca-Fe-Pt-As superconductors are an ideal system for the study of interlayer hopping in the iron-based superconductors using many different techniques. The present detailed ARPES study of the electronic structure of the 10-3-8 phase near the surface serves as an essential first step in that direction.

Work at Princeton is supported by NSF-DMR-1006492 and the AFOSR MURI on superconductivity. The Synchrotron Radiation Center is supported by NSF-DMR-0537588. C. L. acknowledges T. Kondo and A. Kaminski for provision of data analysis software. M. Z. H. acknowledges Visiting Scientist support from LBNL and additional support from the A. P. Sloan Foundation.

[1] K. Kudo *et al.*, International workshop on novel superconductors and super materials, March 6-8, Tokyo, Japan (2011).
[2] N. Ni *et al.*, arXiv:1106.2111 Proc. Natl. Acad. Sci. USA in press (2011).
[3] C. Lohnert *et al.*, arXiv:1107.5320 (2011).

[4] S. Kakiya *et al.*, arXiv:1108.0029 (2011).
[5] Y. Kamihara *et al.*, J. Am. Chem. Soc. **130**, 3296 (2008).
[6] M. Rotter, M. Tegel and D. Johrendt, Phys. Rev. Lett. **101**, 107006 (2008).
[7] D. C. Johnston, Adv. Phys. **59**, 803 (2010).
[8] P. C. Canfield *et al.*, Phys. Rev. B **80**, 060501(R) (2009).
[9] N. Ni and S. L. Bud'ko, MRS bulletin, **36**, 620 (2011).
[10] J. G. Bednorz and K. A. Müller, Z. Phys. B **64**, 189 (1986).
[11] D. M. Ginsberg, Physical Properties of High Temperature Superconductors Vol. V. World Scientific Pub. Co. Inc. ISBN: 978-9810233587 (1996).
[12] A. Mourachkine, High-temperature superconductivity in cuprates: the nonlinear mechanism and tunneling measurements. Springer ISBN: 978-1402008108 (2002).
[13] A. Damascelli, Z. Hussain and Z.-X. Shen, Rev. Mod. Phys. **75**, 473 (2003).
[14] J. C. Campuzano, M. Norman, and M. Randeria, Superconductivity: Physics of Conventional and Unconventional Superconductors, Vol. 1, edited by K. H. Bennemann and J. B. Ketterson (Springer, Berlin, 2008).
[15] D. Hsieh *et al.*, arXiv:0812.2289 (2008).
[16] L. A. Wray *et al.*, Phys. Rev. B **78**, 184508 (2008).
[17] V. B. Zabolotnyy *et al.*, Nature **457**, 569 (2009).
[18] C. Liu *et al.*, Phys. Rev. Lett. **102**, 167004 (2009).
[19] T. Kondo *et al.*, Phys. Rev. B **81**, 060507(R) (2010).
[20] H. Ding *et al.*, J Phys. Condens. Matter **13**, 135701 (2011).
[21] Y. Zhang *et al.*, Nature Materials **10**, 273 (2011).
[22] T. Qian *et al.*, Phys. Rev. Lett. **106**, 187001 (2011).
[23] C. Liu *et al.*, Nature Physics **6**, 419 (2010).
[24] C. Liu *et al.*, Phys. Rev. B **82**, 075135 (2010).
[25] M. Z. Hasan and B. A. Bernevig, Physics **3**, 27 (2010).
[26] G. Kresse, and J. Joubert, Phys. Rev. B **59**, 1758 (1999).
[27] P. E. Blöchl, Phys. Rev. B **50**, 17953 (1994).
[28] G. Kresse and J. Furthmüller, Comput. Mater. Sci. **6**, 15 (1996).
[29] H. Zhai, F. Wang, and D.-H. Lee, Phys. Rev. B **80**, 064517 (2009) and references therein.